# Multi-Shell Porous $TiO_2$ Hollow Nanoparticles for Enhanced Light Harvesting in Dye-sensitized Solar Cells

*Sun Hye Hwang, Juyoung Yun, and Jyongsik Jang**

**An optimized configuration for nanomaterials in working electrodes is vital to the high performance of dye-sensitized solar cells (DSSCs). Here, a fabrication method is introduced for multi-shell $TiO_2$ hollow nanoparticles (MS-$TiO_2$-HNPs) via a sol–gel reaction, calcination, and an etching process. The prepared uniform MS-HNPs have a high surface area (ca. 171 $m^2$ $g^{-1}$), multireflection, and facile electrolyte circulation and diffusion. During the MS-HNP fabrication process, the amount of $SiO_2$ precursor and $H_2O$ under reaction has a significant effect on aggregation and side reactions. The etching process to obtain pure $TiO_2$ is influenced by anatase crystallinity. Additionally, single-shell (SS)-$TiO_2$-HNPs and double-shell (DS)-$TiO_2$-HNPs are synthesized as a control. The MS-$TiO_2$-HNPs exhibit a high surface area and enhance light reflectance, compared with the SS- and DS-$TiO_2$-HNPs of the same size. The power conversion efficiency of the optimized MS-$TiO_2$-HNP-based DSSCs is 9.4%, compared with the 8.0% efficiency demonstrated by SS-$TiO_2$-HNP-DSSCs (a 17.5% improvement). These results enable the utilization of multifunctional MS-HNPs in energy material applications, such as lithium ion batteries, photocatalysts, water-splitting, and supercapacitors.**

## 1. Introduction

The ability to capture sunlight is of great importance for high-performance dye-sensitized solar cells (DSSCs).[1–5] Nano-sized semiconductors, used as the mesoporous layer in DSSCs, have improved the light absorption ability of these solar cells, due to their enhanced surface-to-volume ratio compared with bulk materials.[6–9] However, nanomaterials having a size less than ≈50 nm, such as those used in the DSSC's mesoporous layer, cannot sufficiently scatter or reflect sunlight.[10,11] To overcome these issues, researchers have focused on synthesizing light-scattering materials, such as micro-sized particles,[12] core/shell materials,[13] hierarchical structure materials,[14,15] and nanofibers.[16] However, these light-scattering materials can hinder light absorption in the light-sensitized coating of the mesoporous layer, due to their low surface area. Therefore, efficient light absorption requires consideration of the nanomaterial's size, surface area, and light-scattering ability.

Recently, multi-shell hollow nanoparticles (MS-HNPs) have been highlighted as promising materials for DSSC applications, offering a high surface area and strong light scattering. MS-HNPs, composed of inner and outer shells, have a beneficial configuration for multireflection (of sunlight) and redox reactions with the electrolyte. Moreover, the surface area of MS-HNPs is much larger than that of single-shell (SS)-HNPs having the same size. Various MS-HNPs have been developed, such as multilayerd $SnO_2$ hollow microspheres coated to $TiO_2$,[17] quintuple-shelled $SnO_2$ hollow microspheres,[18] multi-shelled ZnO hollow microspheres,[19] and shell-in-shell $TiO_2$ hollow microspheres.[20] These MS-HNPs improve the power conversion efficiency of the DSSCs, due to their strong light-scattering effect and increased surface area. However, among the MS-HNPs, the largest surface area of multi-shelled ZnO hollow microspheres was only 47 $m^2$ $g^{-1}$, which is not sufficient for light absorption in the sensitizer layer.[19] Additionally, most MS-HNPs are synthesized using a hydrothermal process, which limits the mass production of MS-HNPs. In particular, $TiO_2$, commonly used as the working electrode in DSSCs, has several fabrication issues, including difficulty in controlling the morphology, size, and aggregation, due to the fast reaction rate of the $TiO_2$ precursor.[21,22] Therefore, the development of MS-HNPs with nano-scale size, high surface area, and strong light-scattering remains a challenge.

Herein, we introduce a fabrication method for nano-sized MS-$TiO_2$-HNPs using a sol–gel method, combined with calcination and etching processes. The MS-$TiO_2$-HNPs used in this study were composed of three shells: a small inner shell (diameter: 50 nm), a middle shell (diameter: 100 nm), and an outer shell (diameter: 160 nm). The fabricated MS-$TiO_2$-HNPs were expected to be multifunctional, due to their large surface area of 171 $m^2$ $g^{-1}$, multi-reflection capability, and enhanced electrolyte diffusion. Specifically, the smallest inner shell of the MS-$TiO_2$-HNPs provided a high surface area. Additionally, the multi-shell structure induced multireflection for solar devices. We observed an increase in the power conversion efficiency for the MS-$TiO_2$-HNP-DSSCs of 17.5% (from 8.0% for SS-$TiO_2$-HNP-DSSCs to 9.4% for MS-$TiO_2$-HNP-DSSCs). To our knowledge, this is the first report of nano-sized MS-$TiO_2$-HNPs with a high surface area.

S. H. Hwang, J. Yun, Prof. J. Jang
World Class University (WCU) program
of Chemical Convergence for Energy & Environment ($C_2E_2$)
School of Chemical and Biological Engineering
Seoul National University
599 Gwanangno, Gwanakgu, Seoul 151–742, Korea
E-mail: jsjang@plaza.snu.ac.kr

**DOI: 10.1002/adfm.201401915**

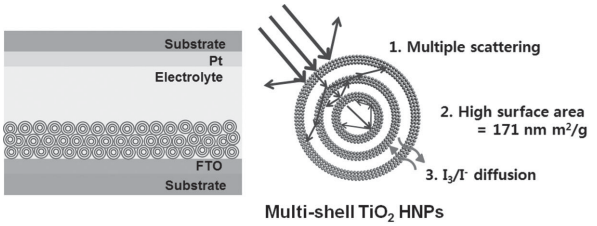


**Figure 1.** Schematic illustration of a) assembled dye-sensitized solar cells (DSSCs) based on multi-shell porous $TiO_2$ hollow nanoparticles (MS-$TiO_2$-HNPs) and b) the magnified structure of MS-$TiO_2$-HNPs with multifunction capabilities.

## 2. Results and Discussion

**Figure 1** shows an illustration of the assembled DSSCs, based on the MS-$TiO_2$-HNPs as the working electrode. The high surface area of the MS-$TiO_2$-HNPs provides additional sites for dye adsorption, thus, effectively improving the light-scattering ability of the MS-$TiO_2$-HNPs, as well as the multiple scattering events between shells. Moreover, the intrawall pores of the MS-$TiO_2$-HNPs facilitate electrolyte diffusion and circulation. **Figure 2** presents a schematic diagram of the fabrication procedure for MS-$TiO_2$-hollow-HNPs. This approach was introduced by our research group in previous studies of $SiO_2/TiO_2$ core/shell nanoparticles (ST-CSNPs).[13,23] In brief, $SiO_2$ colloidal NPs were synthesized using the Stöber method. Titanium (IV) isopropoxide (TTIP) was then introduced to the $SiO_2$ colloidal solution, which was stirred for 12 h at 4 °C. The prepared ST-CSNP solution was washed, dispersed in a 50-mL polyvinylpyrrolidone (PVP: MW = 10 000, 0.3 g) aqueous solution, and stirred for 12 h to allow PVP adsorption to the surface of $TiO_2$ via hydrogen bonding between the carbonyl group of PVP and the hydroxyl groups on $TiO_2$.[24] The PVP-adsorbed ST-CSNPs were then isolated, washed, and redispersed in 79 mL of ethanol under sonication. The redispersed PVP-adsorbed ST-CSNPs in ethanol were mixed with tetraethyl orthosilicate (TEOS), ammonia, and distilled water for 6 h at 38 °C. This created a $SiO_2$ shell on the $TiO_2$ surface via a sol–gel reaction, resulting in the fabrication of $SiO_2/TiO_2/SiO_2/TiO_2$ (STST)-CSNPs. PVP treatment of STST-CSNPs, TEOS mixing with STST-CSNPs, and TTIP dropping to STSTS-CSNPs were performed to fabricate $SiO_2/TiO_2/SiO_2/TiO_2/SiO_2/TiO_2$ (STSTST)-CSNPs. The STSTST-CSNPs were calcinated at 900 °C for 6 h and etched with a NaOH solution (2.5 M, 5 mL), to obtain the anatase crystalline $TiO_2$ phase without the $SiO_2$ phase, thus, creating MS-$TiO_2$-HNPs.

**Figures 3**a–c show transmission electron microscopy (TEM) images of the SS-, double-shell (DS)-, and MS-$TiO_2$-HNPs. The SS-$TiO_2$-HNPs were readily fabricated by adjusting the size of the $SiO_2$ core template to the size of 130 nm. The double-shell (DS) and MS-$TiO_2$-HNPs could also be fabricated by iterations of $SiO_2$ and $TiO_2$ coating processes. The outer diameter of all samples was precisely controlled to obtain a uniform size of ≈160 nm. The red arrows in the Figures indicate the $TiO_2$ shell location (Figure 3). Figure 3a shows uniform, aggregation-free SS-$TiO_2$-HNPs (diameter: 160 nm; shell thickness: 15 nm). The DS-$TiO_2$-HNPs, shown in Figure 3b, exhibited uniform spherical structures (inner diameter: ca. 70 nm; outer diameter: ca. 160 nm); the inner shell was not always located in the center of the HNPs and tended to move within the outer shell. Figure 3c shows the MS-$TiO_2$-HNP structure, with noticeably smaller shells (innermost diameter: ca. 50 nm; middle shell diameter: ca. 100 nm) inside the outer shell (outermost diameter: ca. 160 nm). High-resolution TEM (HR-TEM) shows the mesoporous $TiO_2$ shell composed of small anatase grains (Figure 3d). In the magnified HR-TEM image (inset), the lattice spacing of 0.34 nm matched the anatase crystalline phase of [101] $TiO_2$.[9] The scanning electron microscopy (SEM) image (Figure S1, Supporting Information) shows uniform MS-$TiO_2$-HNPs. From these images, the hollow structure of the $TiO_2$-NPs, as well as its highly porous structure and various numbers of $TiO_2$ shells, was confirmed.

To achieve monodisperse MS-$TiO_2$-HNPs without side reactions, a silica precursor should selectively react with the PVP-adsorbed surface of the ST-CSNPs. The aggregation of STS-CSNPs was dependent on the amount of TEOS added to the solution containing ST-CSNPs. In **Table 1**, large aggregations were observed when more than 5 mL of TEOS was added to the solution containing PVP-adsorbed ST-CSNPs; whereas, no aggregation was evident when less than 4 mL of TEOS was used in this same solution. **Figure 4**a clearly shows a large aggregation of STS-CSNPs when 6 mL of TEOS was added to the reaction solution. To prevent aggregation of the STS-CSNPs during the growth of the $SiO_2$ shell, the sol–gel reaction should be carried out with less than 4 mL of TEOS; at higher TEOS concentrations, the STS-CSNPs grew together during the sol–gel reaction. This was attributed to the short length of the PVP chain (MW: 10 000; hydrodynamic diameter in water: ca. 4 nm).[25,26] After STS-CSNP fabrication, we performed the TTIP coating step to obtain STST-CSNPs

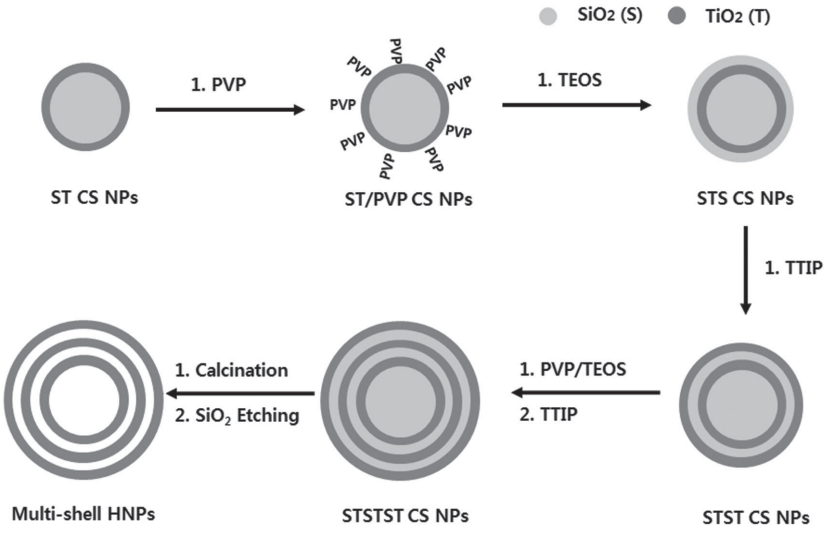


**Figure 2.** Schematic illustration of polyvinylpyrrolidone (PVP) surface modification, $SiO_2$ and $TiO_2$ coating process, and calcination and etching processes for MS-$TiO_2$-HNP fabrication.

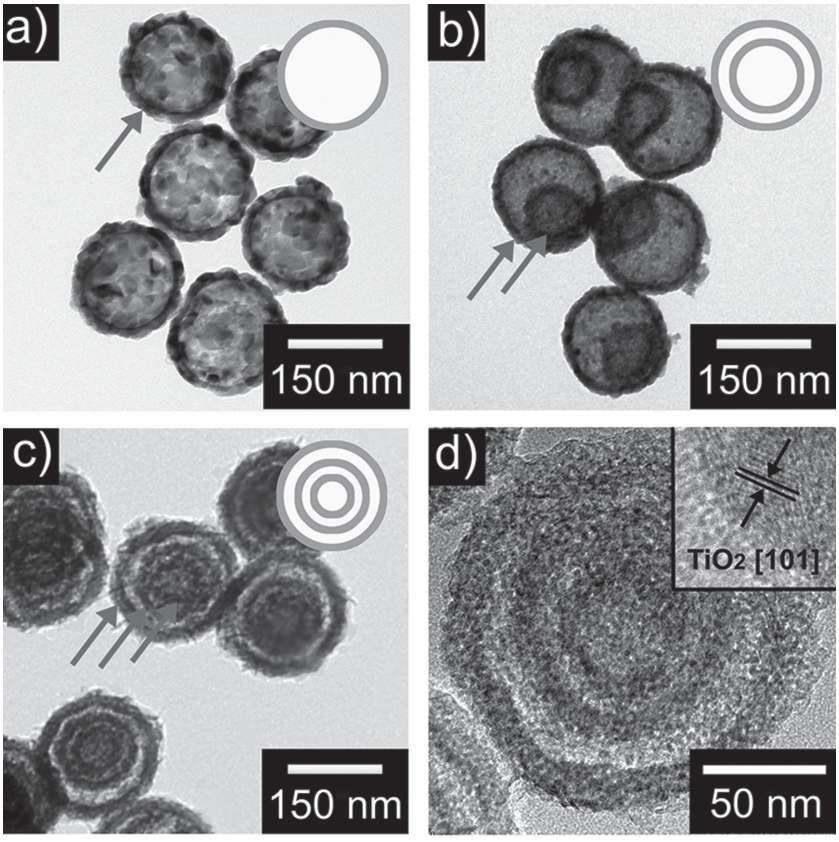


**Figure 3.** Transmission electron microscopy (TEM) images of a) single shell (SS), b) double-shell (DS), and c) MS- $TiO_2$-HNPs. d) High-resolution TEM (HR-TEM) images of MS-$TiO_2$-HNPs (inset: d-spacing of the outer shell of MS-$TiO_2$-HNPs).

without side reactions (i.e., TTIP reacted only with the surface of the STS-CSNPs). The amount of TTIP added was adjusted depending on the expected thickness of the $TiO_2$ shell. If the surface area of the STS-CSNPs per volume was not large enough, compared with the added amount of TTIP, then the formation of small $TiO_2$ nanoparticles from side nucleation of TTIP could be promoted. To overcome side nucleation, Yin et al. reported that the thickness of the $TiO_2$ shell can be controlled by carrying out repeated coating steps.[27] In contrast, we used a simpler method to control the thickness of the $TiO_2$-coated STS-CSNPs, by adjusting the amount of $H_2O$. Table 1 provides information on the solutions containing variable amounts of $H_2O$ in ethanol. In this process, 5-mL TTIP was introduced to a solution containing STS-CSNPs. Side reactions formed small $TiO_2$-NPs when the amount of $H_2O$ was greater than 2.4 mL (Figure 4b). The nucleation of small $TiO_2$-NPs (ca. 20 nm) occurred, due to the fast reaction rate originating from the increased amount of $H_2O$ under the sol–gel reaction.[28] Thus, the amount of TEOS and $H_2O$ play an important role in the fabrication of well-defined STST-CSNPs.

X-ray diffraction (XRD) analysis was carried out to investigate the crystallinity of SS-, DS-, and MS-$TiO_2$-HNPs. **Figure 5**a shows that the DS-$TiO_2$-HNPs calcinated at 600 and 700 °C for 6 h exhibited a broad anatase phase. When calcinated at 800 °C for 6 h, the DS-$TiO_2$-HNPs showed sharp anatase crystalline peaks at $2\theta = 25.3°$, identified as the anatase [101] phase (JCPDS No. 21–1272). We also investigated the optimized calcination temperature to obtain anatase crystallinity of SS-, DS-, and MS-$TiO_2$-HNPs (Figure 5b). For MS-$TiO_2$-HNPs, anatase crystallinity took place at 900 °C; this temperature value was significantly higher than that for the SS- or DS- $TiO_2$-HNPs. In general, the pure anatase phase $TiO_2$ can be obtained in the temperature range of 400–600 °C, while the $TiO_2$ region of SS-, DS-, and MS-$TiO_2$-HNPs initiates transformation to the anatase phase at higher temperatures. According to previous research results, the $TiO_2$ crystallization temperature of the $SiO_2/TiO_2$ composite nanomaterial significantly increased up to 900 °C.[24] The existence of $SiO_2$ at the $TiO_2$ interface acts as a barrier to the diffusion of Ti atoms, leading to delays in nucleation and growth of $TiO_2$ crystallites.[29–31]

To confirm the etching process, we also carried out TEM and SEM/energy dispersive X-ray (SEM/EDX) spectroscopy on

**Table 1.** Summary of sample notation, amount of tetraethyl orthosilicate (TEOS), $H_2O$, and sample morphology of prepared $SiO_2/TiO_2/SiO_2/TiO_2$ (STST).

| Sample notation | TEOS[a] [mL] | $H_2O$[b] $V$ [mL] | Morphology |
|---|---|---|---|
| ST-TEOS3 | 3 | 1.2 | No aggregation |
| ST-TEOS4 | 4 | 1.2 | No aggregation |
| ST-TEOS5 | 5 | 1.2 | Middle aggregation |
| ST-TEOS6 | 6 | 1.2 | High aggregation |
| ST-$H_2O$2.4 | 4 | 2.4 | $TiO_2$ NPs with side rxn |
| ST-$H_2O$6 | 4 | 6 | $TiO_2$ NPs with side rxn |

[a]TEOS solution (25 vol% in EtOH). [b]TTIP/$H_2O$ mixture (vol/vol). rxn: reaction.

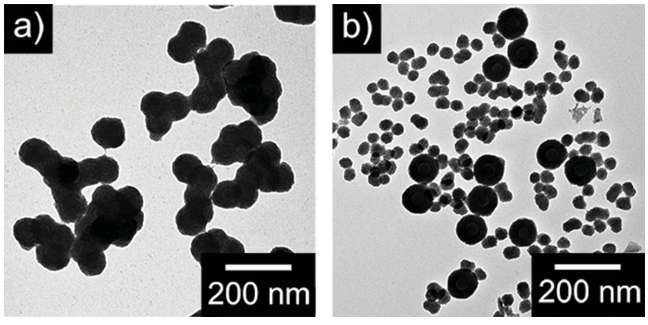


**Figure 4.** TEM images of $SiO_2/TiO_2/SiO_2$-core/shell nanoparticles (STS-CSNPs) prepared by a) 6 mL of tetraethyl orthosilicate (TEOS) added to a solution containing PVP treated ST-CSNPs and b) 5 mL of titanium (IV) isopropoxide (TTIP) added to ethanol-based STS-CSNPs colloidal solution containing 2.4 mL of $H_2O$.

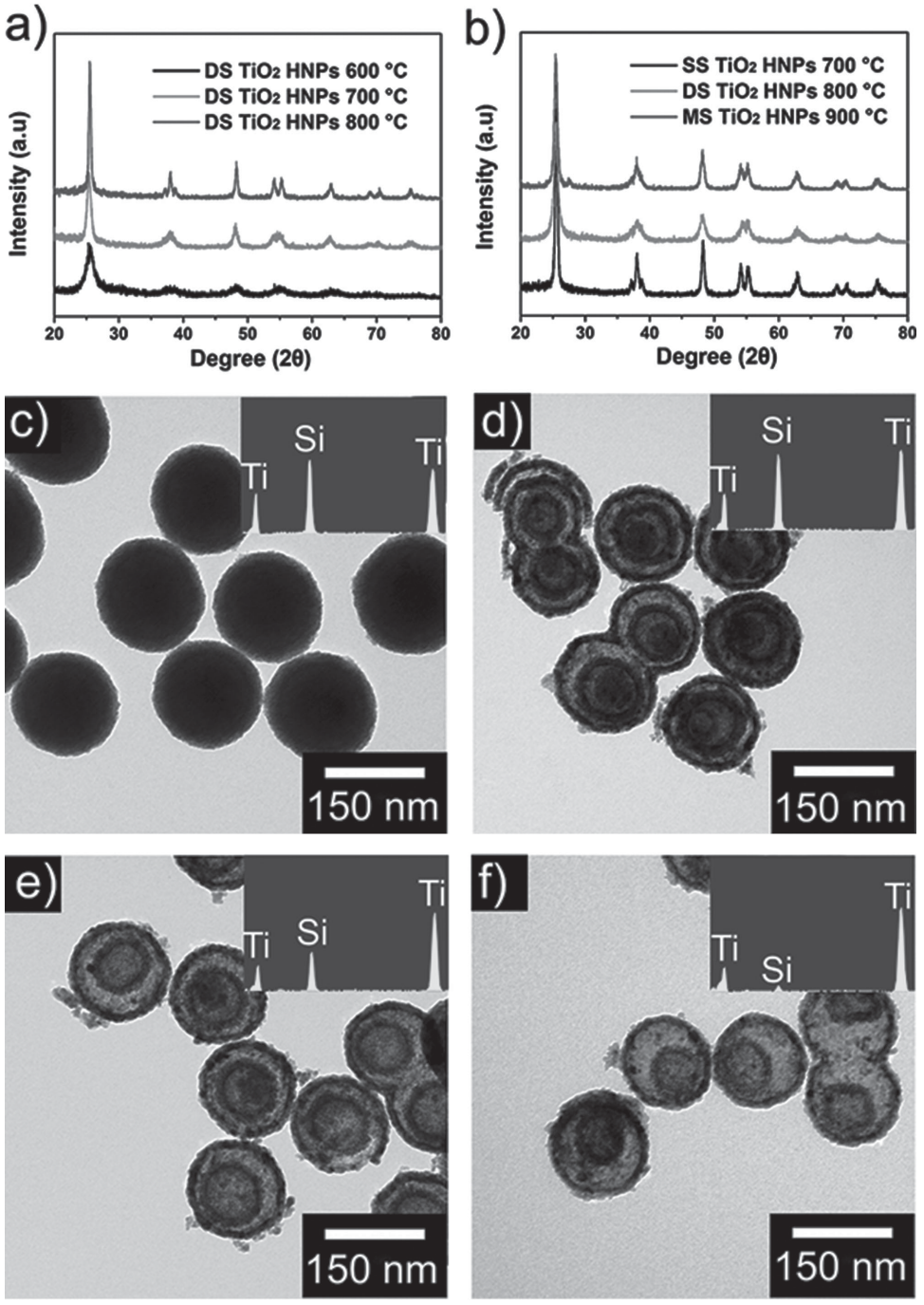


**Figure 5.** X-ray diffraction (XRD) pattern of calcinated samples a) before and b) after NaOH etching. TEM images of the etching process of STST-CSNPs, calcinated at 800 °C for 6 h according to the following etching times: c) 0, d) 12, e) 24, and f) 36 h (500 mg STST-CSNPs in a mixture of 20-mL water and 5-mL NaOH solution (2.5 M) (Inset: Scanning electron microscopy/energy dispersive X-ray (SEM/EDX) spectra of each sample.)

anatase crystalline STST-CSNPs, having undergone etching in a NaOH aqueous solution for different periods of time. The $OH^-$ ions from the NaOH solution can etch $SiO_2$ by coordinating the weakened Si-O bonds and Si atoms, resulting in the formation of a water-soluble silicate species.[32] Figure 5c shows TEM images of STST-CSNPs with uniform diameters of 160 nm. Due to the less compact network of $SiO_2$ at the interface, etching occurred near the $TiO_2$ shell; the inner silica part was more slowly etched, as shown in Figures 5d–f. After 36 h of $SiO_2$ etching, Figure 5f clearly shows pure porous DS-$TiO_2$-HNPs, due to the removal of $SiO_2$. The inset of Figures 5d–f indicated an atomic ratio of Si to Ti of 28:72 (12 h of $SiO_2$ etching), 10:90 (24 h of $SiO_2$ etching), and 3:97 (36 h of $SiO_2$ etching), from SEM/EDX results. In **Table 2**, the low anatase phase of STST-CSNPs (due to calcination at low temperature) did not etch completely, despite 36 h of $SiO_2$ etching. Therefore,

**Table 2.** Summary of sample notation, calcination temperature, crystalline phases, etching hours, and the atomic ratio of Ti:Si.

| Sample notation[a)] | Calcination temperature [°C] | Crystalline phase | Ti:Si weight ratio |
|---|---|---|---|
| 1L_600 | 600 | Anatase | 99:1 |
| 2L_600 | 600 | Low anatase | 72:28 |
| 2L_700 | 700 | Low anatase | 90:10 |
| 2L_800 | 800 | Anatase | 97:3 |
| 3L_700 | 700 | Low anatase | 70:30 |
| 3L_800 | 800 | Low anatase | 90:10 |
| 3L_900 | 900 | Anatase | 97:3 |

[a)]The samples were etched for 36 h in a NaOH aqueous solution.

the calcination temperature and etching hours were important factors in obtaining pure, porous DS-$TiO_2$-HNPs, as well as SS- and MS-$TiO_2$-HNPs.

The synthesized MS-$TiO_2$-HNPs are expected to provide dual functioning: strong light scattering by the multi-layered hollow structure, and increased dye adsorption by the small inner shell. To confirm the light-scattering efficiency of the anode film, diffuse reflectance of SS-, DS-, and MS-$TiO_2$-HNPs was investigated. **Figure 6**a shows that the DS- and MS- HNPs exhibited more effective light reflectance than SS-$TiO_2$-HNPs due to enhanced light scattering, creating strong optical confinement for DSSC anode applications. Previous studies reported that hollow or MS-hollow nanomaterials provided enhanced light scattering due to multireflections.[5,17–20] Recently, Dong et al. determined that the distance between the inner and outer shell of the DS-HNPs influenced their light-scattering efficiency; the closed exterior double shells presented stronger light scattering capability than the normal double shells.[19] Given this outcome, the prepared MS-$TiO_2$-HNPs used in this study had relatively closed shells, compared with the DS-$TiO_2$-HNPs. The slightly higher light-scattering efficiency of MS-$TiO_2$-HNPs may be influenced by the close distance between the inner and outer shell, compared with DS-$TiO_2$-HNPs. We also measured the Brunauer–Emmett–Teller (BET) surface area of SS-, DS-, and MS-$TiO_2$-HNPs using nitrogen adsorption and desorption isotherms (Figure 6b). The BET surface area of MS-$TiO_2$-HNPs was 171.3 $m^2\ g^{-1}$, nearly 2.7 times higher than that of SS-$TiO_2$-HNPs (63.6 $m^2\ g^{-1}$). The surface area of DS-$TiO_2$-HNPs was 128.4 $m^2\ g^{-1}$. The high surface area originated from the inner shell of DS- and MS-$TiO_2$-HNPs, which may facilitate large amounts of dye adsorption on the $TiO_2$ surface. In Figure S2 (Supporting Information), we also measured the pore volume distribution of MS-$TiO_2$-HNPs. The diameter of the intrawall pores in the shells of MS-$TiO_2$-HNPs was 4.09 nm. These pores facilitated electrolyte circulation and diffusion during the oxidation reaction. Figure 6c shows the desorption of dye (N719) from the anode film, composed of SS-, DS-, and MS-$TiO_2$-HNPs, by NaOH. The amount of dye loading on the $TiO_2$ surface increased with increasing surface area of the samples. The amount of desorption of N719 from the surface of MS-$TiO_2$-HNPs was the largest among the samples. From these data, we confirmed that the MS-$TiO_2$-HNPs have the highest

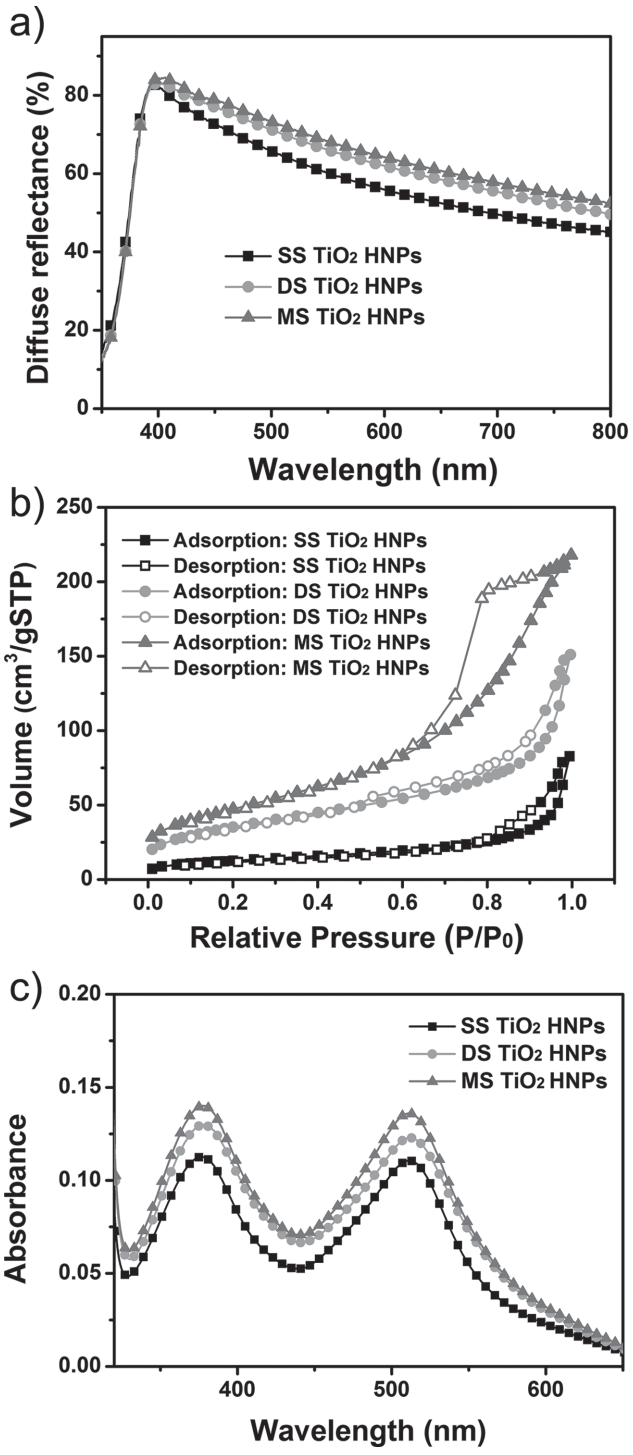


**Figure 6.** a) Diffuse reflectance spectra and b) nitrogen adsorption/desorption isotherms of SS- $TiO_2$-HNPs (square), DS-$TiO_2$-HNPs (circle), and MS-$TiO_2$-HNPs (triangle). c) Dye desorbed from an anode electrode, based on SS-, DS-, and MS-$TiO_2$-HNPs using a NaOH solution (ethanol/water = 1:1, v/v).

light-scattering ability, BET surface area, intrawall pores, and dye loading on the surface of $TiO_2$.

To better understand the influence of SS-, DS-, and MS-$TiO_2$-HNPs on the power conversion efficiency (PCE, $\eta$) of the

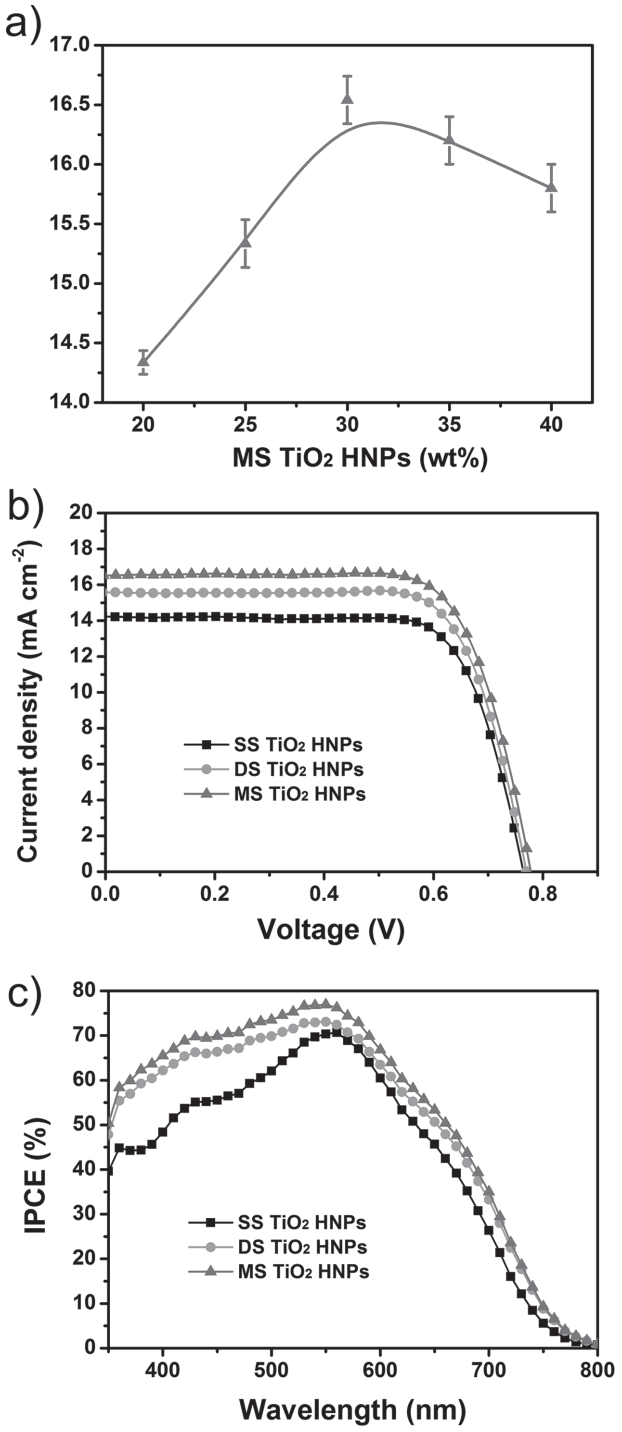


**Figure 7.** Photovoltaic characteristics of a) MS-$TiO_2$-HNPs with different content and b) current density–voltage characteristics (*J–V* curves) and b) incident photon-to-electron conversion efficiencies (IPCE) of SS-, DS-, and MS-$TiO_2$-HNP-based DSSCs.

DSSCs, we measured the current density–voltage (*J–V*) characteristics and incident photon-to-electron conversion efficiencies (IPCEs) of SS-, DS-, and MS-$TiO_2$-HNPs-based DSSCs. **Figure 7**a shows the short-circuit current density ($J_{sc}$) and PCE of DSSCs containing MS-$TiO_2$-HNPs (20–40 wt% content) in the anode film. The PCE of DSSCs increased with increasing MS-$TiO_2$-HNP concentration, up to 30 wt%. However, when the MS-$TiO_2$-HNP concentration was greater than 30 wt%, the PCE decreased slightly. Figure 7b shows an exceptionally high PCE for MS-$TiO_2$-HNPs ($\eta$ = 9.4%), compared with SS- and DS-$TiO_2$-HNP-based DSSCs, with a $J_{sc}$ of 16.54 mA $cm^{-2}$; this $\eta$ value was ca. 17.5% greater than that for SS-$TiO_2$ HNP-DSSCs ($\eta$ = 8.0%). In case of MS-$TiO_2$-HNPs, inner shell and outer shell slightly separate because remained small quantity of silica in HNPs support the separted strucutres. It could be considered that the dye adsored in the inner shell may be delivered to wordking electrode because of the adsence of interconnection. However, MS-$TiO_2$-HNPs were coated with $TiO_2$ thin layer through $TiCl_4$ post-treatment on the photoanode, and the $SiO_2$ bridge could be also coated with $TiO_2$ thin layer, leading to electron transfer between the inner shells and the outer shells. **Table 3** summarizes the photovoltaic parameters from the *J–V* curves. As the number of shells increased from 1 to 3, the $J_{sc}$ and PCE values also increased. The improved performance of the MS-$TiO_2$-HNPs was attributed to two main factors. First, the multi-shell hollow structure made it possible to provide superior light scattering within the DSSC anode, due to multireflection. Second, the surface area of the MS-$TiO_2$-HNPs was 2.7 times higher than that of SS-$TiO_2$-HNPs, providing sufficient dye loading to the surface of $TiO_2$ for light harvesting. To further investigate an effect of $TiO_2$-HNPs on DSSCs, the electrochemical impedance spectroscopy (EIS) was performed as shown in Figure S3 (Supporting Information). The Nyquist plots for DSSCs were measured at –0.77V forward bias in dark condition with a frequency range of 0.1 Hz to 100 kHz. The larger semicircles in Nyquist plots reveal that electron recombination resistance at $TiO_2$/dye/electrolyte interface. The recombination resistance slightly decreased in order of SS-, DS- and MS-$TiO_2$-HNPs, but not quite different. Because MS-$TiO_2$-HNPs has not only an increased surface area which provides more recombination sites, but also has more silica contents retarding charge recombination.[33] Namely, the charge recombination from high surface area offsets the effect of enhancing charge collection by insulating silica contents. Thus, the $V_{oc}$ of the three cells are almost same. As shown in Figure 7c, IPCEs were measured to confirm the effect of SS-, DS-, and MS-$TiO_2$-HNPs on the spectral response. The DS- and MS-$TiO_2$-HNPs exhibited enhanced quantum efficiency at both short and long wavelengths, compared with SS-$TiO_2$-HNPs. The IPCE of MS-$TiO_2$-HNPs increased from 48.3 to 65.4% at 400 nm (short

**Table 3.** Summary of the current density–voltage characteristics of SS, DS, and MS-$TiO_2$-HNP-based anode electrode of DSSCs.

| Sample[a)] | $J_{sc}$[b)] [mA $cm^{-2}$] | $V_{oc}$[c)] [V] | FF[d)] | $\eta$[e)] [%] |
|---|---|---|---|---|
| SS $TiO_2$ HNPs | 14.23 | 0.77 | 0.74 | 8.0 |
| DS $TiO_2$ HNPs | 15.57 | 0.77 | 0.74 | 8.9 |
| MS $TiO_2$ HNPs | 16.52 | 0.77 | 0.73 | 9.4 |

[a)]Active area of the assembled DSSC samples is 0.16 $cm^2$; [b)]Short-circuit current density; [c)]Open-circuit voltage; [d)]Fill factor; [e)]Power conversion efficiency; SS: single-shell; DS: double-shell; MS: multi-shell; DSSC: dye-sensitized solar cell; MS-$TiO_2$-HNPs: multi-shell $TiO_2$ hollow nanoparticles.

wavelength), corresponding to ≈35.5%, compared with SS-$TiO_2$-HNPs. Additionally, at 650 nm, the IPCE of MS-$TiO_2$-HNPs improved from 45.7% to 53.3% at 650 nm (long-wavelength). The improved light absorption at short wavelengths was attributed to the increased surface area; whereas, light absorption at long wavelengths was induced by enhanced light scattering by the multi-shell hollow structure of DS- and MS-$TiO_2$-HNPs. Thus, our results indicate the suitability of MS-$TiO_2$-HNPs for the full spectrum of solar energy.

## 3. Conclusions

In summary, MS-$TiO_2$-HNPs were successfully fabricated using the sol–gel reaction, calcination, and etching with a NaOH solution. The amount of TEOS and $H_2O$ was adjusted to fabricate well-defined MS-$TiO_2$-HNPs. The calcination temperature also played an important role in the formation of anatase crystallinity of the $TiO_2$ region. The temperature for the anatase phase of $SiO_2$/$TiO_2$ composite materials was much higher than that of $TiO_2$, due to the barriers to Ti-atom diffusion by the $SiO_2$ region. The etching conditions were optimized to obtain the pure $TiO_2$ phase. Additionally, MS-$TiO_2$-HNPs provided multi-reflectance, high surface area, and facile electrolyte diffusion and circulation, leading to an increased current density in the anode electrode. As a result, the PCE of MS-$TiO_2$-HNP-based DSSCs improved to 9.4%, compared with 8.0% for SS-$TiO_2$-HNP-based DSSCs (ca. 17.5% improvement). The MS-$TiO_2$-HNP configuration is expected to play an important role in photocatalyst, lithium-ion battery, supercapacitor, drug delivery, and electrorheological fluid applications.

## 4. Experimental Section

*Synthesis of Multi-Shell (MS)-$TiO_2$-HNPs*: Silica nanoparticles were synthesized via the Stöber method. A mixture of titanium (IV) isopropoxide (TTIP), ethanol, and acetonitrile was added to the prepared colloidal silica solution, initiating a sol–gel reaction at 4 °C for 6 h. The TTIP-added silica nanoparticles were transformed into silica/titania core/shell nanoparticles (ST-CSNPs). The resulting product, ST-CSNPs, was obtained by centrifugation at 10 000 rpm for 30 min, and then redispersed in 40 mL of deionized water. The solution containing fully dispersed ST-CSNPs was stirred with polyvinylpyrrolidone (PVP) (MW: 10 000; 300 mg) overnight to allow PVP to adsorb to the surface of the ST-CSNPs, which were then centrifuged and redispersed in 79 mL of ethanol. The solution was then mixed with 0.7 mL of deionized water and 1 mL of ammonia solution. Tetraethyl orthosilicate (TEOS) (4.5 mL) was added to the above colloidal solution and stirred at 38 °C for 12 h. After the formation of the $SiO_2$ shell on the surface of the ST-CSNPs, 4.5 mL of TTIP, 9 mL of ethanol, and 3 mL of acetonitrile were added to the colloidal solution. The sol–gel reaction produced silica/titania/silica/titania core/shell nanoparticles (STST-CSNPs). To obtain silica/titania/silica/titania/silica/titania core/shell nanoparticles (STSTST-CSNPs), the coating process of silica and titania was repeated once more; the resulting product (STSTST-CSNPs) was obtained by centrifugation at 10 000 rpm for 10 min, which was then washed with ethanol and oven-dried under vacuum. The STSTST-CSNPs were then calcinated at 900 °C for 6 h. The prepared STSTST-CSNPs were etched by various concentrations of NaOH solution to obtain multi-shell (MS)-$TiO_2$-HNPs. To obtain the anatase crystalline $TiO_2$ phase, the $SiO_2$ part of the anatase-phase STSTST-CSNPs, dispersed in 20 mL of distilled water, was etched with an NaOH solution (2.5 M, 5 mL).

*Assembly of Dye-sensitized Solar Cells (DSSCs)*: SS-, DS-, or MS-$TiO_2$-HNPs were added to a terpineol-based paste, and then mixed using a mortar and pestle (paste: sample 70:30 wt/wt) to make a sample paste. Fluorine-doped tin dioxide (FTO) glass substrates were cleaned by successive sonication in deionized water, acetone, and 2-propanol for 60 min each, and then treated with oxygen plasma for 30 s. The FTO glass substrate was pretreated with a 40-mM $TiCl_4$ solution and heated at 450 °C for 30 min. The photoanode was fabricated by applying the previously prepared SS-, DS-, or MS-$TiO_2$-HNPs paste to the FTO substrate, using a screen print. The photoanodes were sintered at 450 °C for 30 min, and then treated with $TiCl_4$ and sintered again as above. The resulting $TiO_2$ films were immersed in absolute ethanol containing $5 \times 10^{-4}$ M of N719 and kept at room temperature for 18 h. Pt counterelectrodes were prepared on the FTO substrates using a 5-mM $H_2PtCl_6$ solution, followed by heating at 400 °C for 30 min in air. The electrolyte in the sealed cell was an $I^-/I^{3-}$ redox couple containing 0.60-M BMII, 0.1-M LiI, 0.05-M $I_2$, and 0.5-M *t*-butylpyridine in acetonitrile.

*Instruments*: The morphology of the SS-, DS-, and MS-$TiO_2$-HNPs was investigated by transmission electron microscopy (TEM, JEM-200CX; JEOL) and field-emission scanning electron microscopy (FE-SEM, 6700; JEOL, Tokyo, Japan) equipped with an energy dispersive X-ray spectroscopy (EDS) system. X-ray diffraction (XRD) data were measured using an M18XHF-SRA (Mac Science Co., Yokohama, Japan) with a Cu-K$\alpha$ radiation source ($\lambda$ = 1.5406 Å) at 40 kV and 300 mA (12 kW). Brunauer–Emmett–Teller (BET) surface areas of HNPs were obtained using a Micromeritics surface area analyzer (ASAP 2000; Micromeritics Co., Norcross, GA). Ultraviolet-visible (UV–Vis) diffuse reflectance spectroscopy (DRS) and UV–Vis absorption spectroscopy were performed using the Lambda 35 system (Perkin-Elmer). The photocurrent–voltage (*I*–*V*) characteristics of the assembled SS-, DS-, and MS-$TiO_2$-HNP-based DSSCs were measured using a 500-W xenon lamp (XIL model 05A50KS source units). The incident photon-to-current efficiency (IPCE; PV Measurements, Inc., Boulder, CO) was evaluated over the range of 300 to 800 nm, under a global AM 1.5 solar emission spectrum.

## Supporting Information

Supporting Information is available from the Wiley Online Library or from the author.

## Acknowledgements

This work was supported by Global Frontier R&D Program on Center for Multiscale Energy System funded by the National Research Foundation under the Ministry of Education, Science and Technology, Korea (2011–0031573)

Received: June 11, 2014
Revised: August 7, 2014
Published online: October 6, 2014

[1] A. Hagfeldt, G. Boschloo, L. Sun, L. Kloo, H. Pettersson, *Chem. Rev.* **2010**, *110*, 6595.
[2] B. O'Regan, M. Grätzel, *Nature* **1991**, *353*, 737.
[3] M. Grätzel, *Inorg. Chem.* **2005**, *44*, 6841.
[4] A. Yella, H. W. Lee, H. N. Tsao, C. Yi, A. K. Chandiran, M. K. Nazeeruddin, E. W. G. Diau, C. Y. Yeh, S. M. Zakeeruddin, M. Grätzel, *Science* **2011**, *334*, 629.
[5] S. H. Hwang, D. H. Shin, J. Yun, C. Kim, M. Choi, J. Jang, *Chem. Eur. J.* **2014**, 20, 4439.
[6] D. Chen, F. Huang, Y. B. Cheng, R. A. Caruso, *Adv. Mater.* **2009**, *21*, 2206.

[7] Q. Zhang, G. Cao, *Nano Today* **2011**, *6*, 91.
[8] L. Hu, S. Dai, J. Weng, S. Xiao, Y. Sui, Y. Huang, S. Chen, F. Kong, X. Pan, L. Liang, K. Wang, *J. Phys. Chem. B* **2007**, *111*, 358.
[9] S. H. Hwang, C. Kim, H. Song, S. Son, J. Jang, *ACS Appl. Mater. Interfaces* **2012**, *4*, 5287.
[10] P. Joshi, L. Zhang, D. Davoux, Z. Zhu, D. Galipeau, H. Fong, Q. Qiao, *Energy Environ. Sci.* **2010**, *3*, 1507.
[11] H. J. Koo, Y. J. Kim, Y. H. Lee, W. I. Lee, K. Kim, N. G. Park, *Adv. Mater.* **2008**, *20*, 195.
[12] I. G. Yu, Y. J. Kim, H. J. Kim, C. Lee, W. I. Lee, *J. Mater. Chem.* **2011**, *21*, 532.
[13] S. Son, S. H. Hwang, C. Kim, J. Y. Yun, J. Jang, *ACS Appl. Mater. Interfaces* **2013**, *5*, 4815.
[14] J. Qu, G. R. Li, X. P. Gao, *Energy Environ. Sci.* **2010**, *3*, 2003.
[15] W. Q. Wu, Y. F. Xu, H. S. Rao, C. Y. Su, D. B. Kuang, *J. Am. Chem. Soc.* **2014**, *136*, 6437.
[16] L. Yang, W. W. F. Leung, *Adv. Mater.* **2011**, *23*, 4559.
[17] J. Qian, P. Liu, Y. Xiao, Y. Jiang, Y. Cao, X. Ai, H. Yang, *Adv. Mater.* **2009**, *21*, 3663.
[18] Z. Dong, H. Ren, C. M. Hessel, J. Wang, R. Yu, Q. Jin, M. Yang, Z. Hu, Y. Chen, Z. Tang, H. Zhao, D. Wang, *Adv. Mater.* **2014**, *26*, 905.
[19] Z. Dong, X. Lai, J. E. Halpert, N. Yang, L. Yi, J. Zhai, D. Wang, Z. Tang, L. Jiang, *Adv. Mater.* **2012**, *24*, 1046.
[20] X. Wu, G. Q. Lu, L. Wang, *Energy Environ. Sci.* **2011**, *4*, 3565.
[21] X. Chen, S. S. Mao, *Chem. Rev.* **2007**, *107*, 2891.
[22] H. Yin, Y. Wada, T. Kitamura, S. Kambe, S. Murasawa, H. Mori, T. Sakata, S. Yanagida, *J. Mater. Chem.* **2001**, *11*, 1694.
[23] C. Kim, M. Choi, J. Jang, *Catal. Commun.* **2010**, *11*, 378.
[24] J. B. Joo, Q. Zhang, M. Dahl, I. Lee, J. Goebl, F. Zaera, Y. Yin, *Energy Environ. Sci.* **2012**, *5*, 6321.
[25] C. Graf, D. L. J. Vossen, A. Imhof, A. Van Blaaderen, *Langmuir* **2003**, *19*, 6693.
[26] M. Pattanaik, S. K. Bhaumik, *Mater. Lett.* **2000**, *44*, 352.
[27] J. B. Joo, Q. Zhang, I. Lee, M. Dahl, F. Zaera, Y. Yin, *Adv. Funct. Mater.* **2012**, *22*, 166.
[28] A. J. Maira, K. L. Yeung, C. Y. Lee, P. L. Yue, C. K. Chan, *J. Catal.* **2000**, *192*, 185.
[29] R. M. Almeida, E. E. Christensen, *J. Sol-Gel Sci. Technol.* **1997**, *8*, 409.
[30] S. M. Melpolder, A. W. West, C. L. Barnes, T. N. Blanton, *J. Mater. Sci.* **1991**, *26*, 3585.
[31] B. Louis, N. Krins, M. Faustini, D. Grosso, *J. Phys. Chem. C* **2011**, *115*, 3115.
[32] S. J. Park, Y. J. Kim, S. J. Park, *Langmuir* **2008**, *24*, 12134.
[33] H. J. Son, X. Wang, C. Prasittichai, N. C. Jeong, T. Aaltonen, R. G. Gordon, J. T. Hupp, *J. Am. Chem. Soc.* **2012**, *134*, 9537.